10.4 EFFECT OF NITRIC ACID ON DROPLET GROWTH AND EVAPORATION: EXPERIMENTAL VALIDATION OF MODELING STRATEGIES

Huiwen Xue and Dennis Lamb *
Department of Meteorology, The Pennsylvania State University, University Park, PA 16802

1. INTRODUCTION

Nitric acid, a highly soluble trace gas generated in the atmosphere by photochemical processes, affects the behavior of aerosol and cloud particles because of its strong affinity for water. The lowered water activity of solution droplets containing nitric acid enhances their condensational growth and retards their evaporation (Lamb 1992, Kulmala et al. 1997, Laaksonen et al. 1998, Charlson et al. 2001). Several numerical models have recently included the water-nitric acid interaction to demonstrate the impacts nitric acid uptake can have on cloud formation, the chemical properties and microstructure of aerosols, and particle lifetimes (Kulmala et al. 1993, Meilinger et al. 1995, Laaksonen et al. 1997, Hegg 2000). However, the modeling of such phenomena involves several fundamental assumptions regarding both the kinetics of particle growth and the chemical equilibria in concentrated solutions.

This study provides some much-needed verification of the physics underlying the phenomena. Droplets in the radius range of 15-30 μm were launched into a gaseous environment that was intentionally out of equilibrium with the droplet properties in order to learn quantitatively how they adjust to new conditions. The time-dependent sizes of the droplets were measured to high precision via Mie-scattering techniques and compared with calculations from a kinetic mass growth model coupled to a chemical thermodynamic model.

2. THEORY OF DROPLET GROWTH

The mass rate of change of each volatile component in a solution droplet in a steady state vapor field is commonly given as (Pruppacher and Klett 1997, p. 506)

$$\frac{dm_i}{dt} = \frac{4\pi a D^*_{v,i} M_i}{R}\left(\frac{p_{\infty,i}}{T_\infty} - \frac{p_{sat,i}}{T_a}\right), \quad (1)$$

where i = 1 for H_2O, and i = 2 for HNO_3 in this study, a is the droplet radius, T_∞ is the ambient temperature, T_a is the droplet temperature, R is the universal gas constant, m_i, M_i, $p_{\infty,i}$, $p_{sat,i}$, and $D^*_{v,i}$ are, respectively, the aqueous-phase mass, molar mass, ambient partial pressure, equilibrium vapor pressure, and effective gas-phase diffusion coefficient (including surface kinetic effects) for component i.

Under the assumption that the enthalpy of H_2O condensation is in balance with the thermal energy conducted away by the surrounding gas (neglecting the enthalpy of HNO_3 condensation), the droplet temperature may be expressed in the form of (Pruppacher and Klett 1997, p. 509)

$$T_a = T_\infty + \frac{L_e}{4\pi a k^*_g}\cdot\frac{dm_1}{dt}, \quad (2)$$

where L_e is the specific enthalpy of H_2O evaporation and k^*_g is the effective thermal conductivity of the surrounding gas (including surface kinetic effects).

In Equations (1) and (2), $D^*_{v,i}$ and k^*_g have the forms of (Pruppacher and Klett 1997, p. 506, p. 509)

$$D^*_{v,i} = \frac{D_{v,i}}{\frac{a}{a+\Delta} + \frac{4D_{v,i}}{a\alpha_i \bar{v}_i}}, \quad (3)$$

$$k^*_g = \frac{k_g}{\frac{a}{a+\Delta} + \frac{4k_g}{a\alpha_T n_g C_p \bar{v}}}, \quad (4)$$

where $D_{v,i}$, α_i, and $\bar{v}_i$ are, respectively, the diffusion coefficient, mass accommodation coefficient, and mean molecular speed of component i, Δ is a distance on the order of one mean free path from the droplet surface, k_g, n_g, C_p, and $\bar{v}$ are, respectively, the thermal conductivity, number density, heat capacity, and mean molecular speed of the ambient gas, while α_T is the thermal accommodation coefficient. Variables m_1, m_2, and T_a are the primary unknowns to be solved from Equations (1) and (2). The droplet radius, a, is related to m_1, m_2, and T_a through a density calculation (e.g., Luo et al. 1996). The equilibrium vapor pressures, $p_{sat,1}$ and $p_{sat,2}$, are related to m_1, m_2, and T_a through the chemical equilibria in solution, such as calculated by the thermodynamic model developed by Carslaw et al. (1995) for a multicomponent system. In their chemical model, the activity coefficients of H_2O, cations, and anions in the mixtures are derived through an ion-interaction approach. The time-dependent droplet mass, composition, and size were calculated for the specific experimental conditions in this study.

3. EXPERIMENTAL METHODS

Charged droplets, derived from bulk solutions of "Ultrapure" reagents (J. T. Baker), were levitated in a cubic electrodynamic cell (Lamb et al. 1996). A single droplet was trapped by the AC electrical field for each experimental run and exposed to a steady horizontal, laminar flow of N_2 containing known concentrations of

* Corresponding author address: Dennis Lamb, 503 Walker Building, Penn State University, University Park, PA 16802, USA; email: lno@ems.psu.edu.

H_2O and HNO_3 vapors. The droplet was illuminated with an argon-ion laser (0.488 μm) so that both its focused image and Mie interference patterns were obtained simultaneously (see Fig. 1).

The radius of the droplet at one instant during the evaporation (or growth) was determined with an absolute error less than ±0.5 μm by adjusting the size parameter in the Mie scattering calculation (Fig. 1) to produce the same number of fringes as observed in a given angular range of view. This size was used as a reference for determining radii at other times by an integration method, which takes account of the property that the overall intensity of the scattered light over the entire angle range attains a maximum for every 0.063-μm change in droplet radius for our optical setup (note line segments in Fig. 2). The change in droplet size within a certain time period can be determined to high precision (±0.03 μm) by counting the number of overall intensity maxima observed in that period. An average refractive index (1.35) was used because the Mie scattering properties are not sensitive to the refractive index over the range of conditions covered in this study (Luo et al. 1996).

Some variables that need to be specified in the model calculations were evaluated through the experiments. The initial droplet composition was known from the bulk solution used, and the initial size was determined by extrapolation of the measured sizes in the early stage to time zero. The temperature of the gas entering the cell was measured with a thermocouple referenced to a platinum-resistance thermometer (±0.02 °C; Omega), while the humidity was measured with a dew point hygrometer (±0.2 °C; General Eastern). The gas-phase HNO_3 concentration was determined by sampling the gas exiting the cell with a nylon tubing and ultrasonically extracting the accumulated HNO_3 in a weak bicarbonate solution that was later analyzed for NO_3^- by ion chromatography. The diffusion coefficient of H_2O was taken from Pruppacher and Klett (1997, p. 503) and that of HNO_3 was based on Graham's law. The thermal accommodation coefficient was set at 0.7 (Shaw and Lamb 1999). The mass accommodation coefficient of H_2O was used as a free parameter to best fit the data in the early stage of droplet evaporation when H_2O mass transfer dominates. By minimizing the standard deviation, the best-fit H_2O accommodation coefficient and dew point (within the experimental error) were found. With these values known, the mass accommodation coefficient of HNO_3 was used as a free parameter to fit the data toward the end of the binary evaporation experiments.

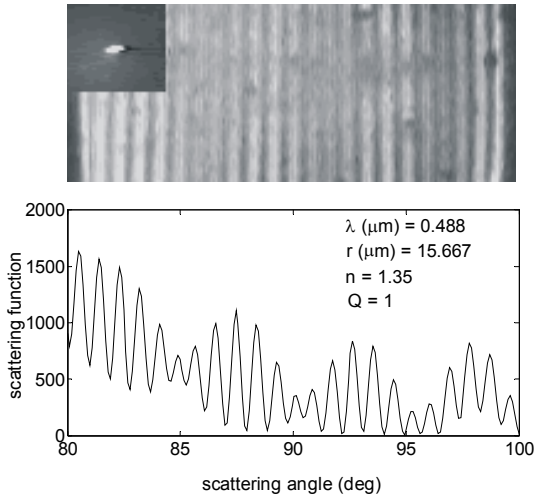

Fig. 1. Upper panel: Video image of the Mie interference fringes from a solution droplet between scattering angles of 80° and 100°. The inset is a focused image of the droplet. Lower panel: Theoretical calculation of the Mie scattering function, with the same number of fringes as shown in the image in the upper panel. The refractive index of the droplet is 1.35, and the droplet radius is 15.667 μm, while the light wavelength is 0.488 μm. Q = 1 represents incident light that is polarized parallel to the scattering plane.

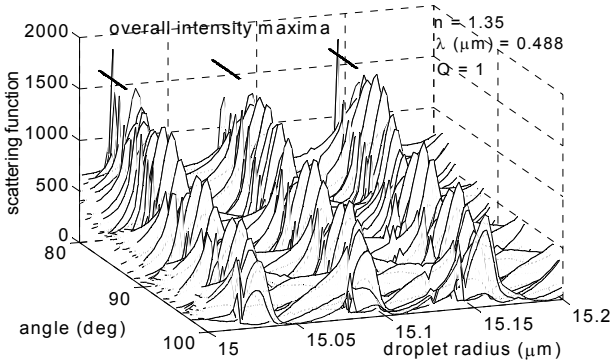

Fig. 2. Theoretical calculation of the Mie scattering function as a function of scattering angle and droplet radius. The scattering function exhibits periodic maxima along the axis of scattering angle, as well as along the axis of the droplet radius.

4. RESULTS AND DISCUSSION

The initial droplet compositions and the ambient conditions for several representative experiments are shown in Table 1. The experimental results for binary HNO_3/H_2O solution droplets are shown in Figure 3 and those for ternary $H_2SO_4/HNO_3/H_2O$ solution droplets are shown in Figure 4. Model calculations of droplet size based on Equations (1) and (2) are shown by the various curves in Figures 3 and 4, with the equilibrium vapor pressures determined from Carslaw et al. (1995) and the density calculated from Luo et al. (1996). The mass accommodation coefficient of H_2O is found to be 0.03-0.05 and that of HNO_3 to be 0.1-0.2 by best-fitting the data for binary HNO_3/H_2O solution droplets.

Table 1. Initial droplet compositions, ambient temperatures, relative humidities, HNO_3 vapor mixing ratios for the experiments at atmospheric pressure.

Droplet	H_2SO_4 wt%	HNO_3 wt%	H_2O wt%	T, °C	RH, %	HNO_3 ppmv
1	0	29.0	71.0	25.1	82.9	0
2	0	5.6	94.4	23.03	88.8	0
3	0	5.6	94.4	-30.94	0	0
4	6.2	3.5	90.3	23.89	88.1	0
5	6.6	0	93.4	23.00	77.0	4.1

Two stages of evaporation (or growth) can be defined based on the different time scales of H_2O and HNO_3 to approach equilibrium. During the first stage, when the transient growth of droplet 1 and the fast evaporation of droplets 2 and 3 take place, H_2O exchanges rapidly between the droplets and their gaseous environments to approach equilibrium. (Calculations indicate that the mass fluxes of H_2O are much larger than those of HNO_3 in this stage.) The second stage of evaporation starts when the H_2O and HNO_3 mass fluxes are comparable and proportionate. The slow mass transfer of HNO_3 is the limiting factor for droplet evaporation in this stage, thus the cause of significant prolongation of droplet lifetimes compared to pure water droplets under the same conditions.

The evaporation (or growth) of ternary $H_2SO_4/HNO_3/H_2O$ droplets exhibits similar features as binary HNO_3/H_2O solution droplets. Large mass transfer of H_2O takes place in the first stage of evaporation. In the second stage, the evaporation of droplet 4 is limited by the slow desorption of aqueous-phase HNO_3, whereas droplet 5, initially devoid of HNO_3, actually starts to grow in response to the uptake of HNO_3 from the gas phase. The importance of HNO_3 in affecting the behavior of sulfate particles during the second stage of evaporation (or growth) is clearly indicated by comparison with the evaporation of H_2SO_4/H_2O droplets in the absence of HNO_3 (thin curves in Fig. 4). However, compared to binary HNO_3/H_2O solution droplets that totally evaporate, the ternary $H_2SO_4/HNO_3/H_2O$ solution droplets approach their equilibrium states after HNO_3 gradually equilibrates in the second stage.

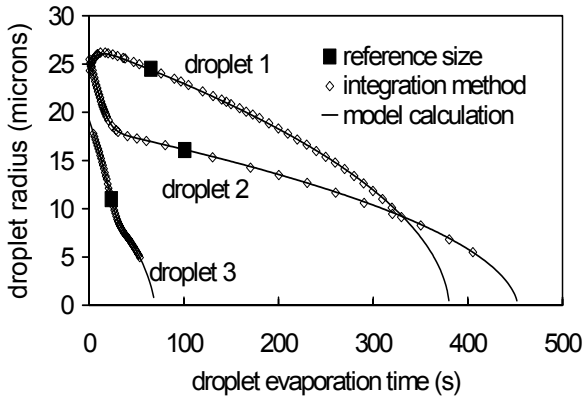

Fig. 3. Measured and calculated sizes for HNO_3/H_2O droplets under conditions given in Table 1.

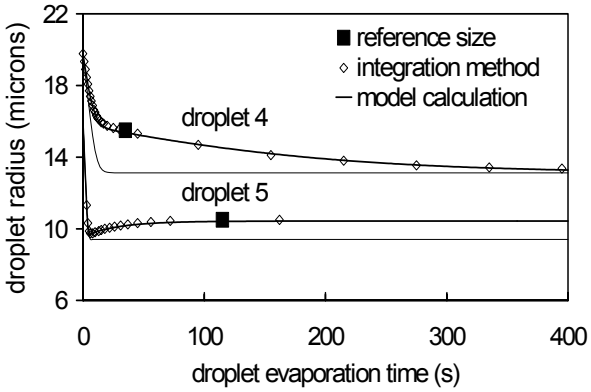

Fig. 4. Measured and calculated sizes for $H_2SO_4/HNO_3/H_2O$ droplets under conditions given in Table 1. The thin curves are evaporation/growth curves for H_2SO_4/H_2O droplets with no HNO_3 present in the system, but H_2SO_4 masses and other conditions same as droplets 4 and 5.

5. CONCLUSIONS

The results demonstrate that the calculated droplet sizes fit the data extremely well, thus validating the coupling of a detailed model of droplet chemistry with a commonly used kinetic model for mass and energy transfer. The model, once validated, serves as a valuable diagnostic tool that helps us understand the changing properties of the droplets. We find that adjustment to new environmental conditions occurs in two stages, one dictated by the transport of water, the other by the exchange of nitric acid. The overall kinetics of droplet evaporation and growth is, however, limited by the presence of the nitric acid, which equilibrates slowly compared to water. Future work will be focused on investigating the effects of HNO_3 on the freezing of solution droplets and the evaporation of solid solution particles under conditions similar to those in the upper troposphere and lower stratosphere.

ACKNOWLEDGMENTS

This research was supported by the National Science Foundation under grant ATM-9981511. We are grateful to S. L. Clegg for providing the code for the chemical thermodynamic model and to A. M. Moyle for technical assistance with the experiments.

REFERENCES

Carslaw, K. S., S. L. Clegg, and P. Brimblecombe, 1995: A thermodynamic model of the system HCl-HNO_3-H_2SO_4-H_2O, including solubilities of HBr, from <200 to 328 K. *J. Phys. Chem.*, **99**, 11,557-11,574.

Charlson, R. J., J. H. Seinfeld, A. Nenes, M. Kulmala, A. Laaksonen, and M. C. Facchini, 2001: Reshaping the theory of cloud formation. *Science*, **292**, 2025-2026.

Hegg, D. A., 2000: Impact of gas-phase HNO_3 and NH_3 on microphysical processes in atmospheric clouds. *Geophys. Res. Lett.*, **27**, 2201-2204.

Kulmala, M., A. Laaksonen, P. Korhonen, T. Vesala, and T. Ahonen, 1993: The effect of atmospheric nitric acid vapor on cloud condensation nucleus activation. *J. Geophys. Res.*, **98**, 22,949-22,958.

Kulmala, M., A. Laaksonen, R. J. Charlson, and P. Korhonen, 1997: Clouds without supersaturation. *Nature*, **388**, 336-337.

Laaksonen, A., J. Hienola, M. Kulmala, and F. Arnold, 1997: Supercooled cirrus cloud formation modified by nitric acid pollution of the upper troposphere. *Geophys. Res. Lett.*, **24**, 3009-3012.

Laaksonen, A., P. Korhonen, M. Kulmala, and R. J. Charlson, 1998: Modification of the Kohler equation to include soluble trace gases and slightly soluble substances. *J. Atmos. Sci.*, **55**, 853-862.

Lamb, D., 1992: Microphysical and chemical aspects of cloud formation at low temperatures. *Proceedings, 11th International Conference on Clouds and Precipitation*, Montreal, Canada, 869-872.

Lamb, D., A. M. Moyle, and W. H. Brune, 1996: The environmental control of individual aqueous particles in a cubic electrodynamic levitation system. *Aerosol Sci. Technol.*, **24**, 263-278.

Luo, B., U. K. Krieger, and Th. Peter, 1996: Densities and refractive indices of H_2SO_4/HNO_3/H_2O solutions to stratospheric temperatures. *Geophys. Res. Lett.*, **23**, 3707-3710.

Meilinger, S. K., T. Koop, B. P. Luo, T. Huthwelker, K. S. Carslaw, U. Krieger, P. J. Crutzen and Th. Peter, 1995: Size-dependent stratospheric droplet composition in lee wave temperature fluctuations and their potential role in PSC freezing. *Geophys. Res. Lett.*, **22**, 3031-3034.

Pruppacher, H. R., and J. D. Klett, 1997: *Microphysics of Clouds and Precipitation*, 954 pp., Kluwer Academic Publishers.

Shaw, R. A., and D. Lamb, 1999: Experimental determination of the thermal accommodation and condensation coefficients of water. *J. Chem. Phys.*, **111**, 10,659-10,663.